DOI: 10.4408/IJEGE.2011-03.B-051

QUASI-THREE DIMENSIONAL TWO-PHASE DEBRIS FLOW MODEL ACOUNTING FOR BOULDER TRANSPORT

C.E. MARTINEZ(*), F. MIRALLES-WILHELM(**) & R. GARCIA-MARTINEZ(***)

(*) Department of Civil and Environmental Engineering, Florida International University
(**) Department of Earth and Environment, Florida International University
(***) Department of Earth and Environment, Florida International University and FLO-2D Software, Inc

ABSTRACT

We present a quasi three-dimensional numerical model to simulate debris flows accounting for a continuum non-Newtonian fluid phase composed by water and fine sediments, and a non-continuum phase for large particles such as boulders. Particles are treated in a Lagrangian frame of reference using the 3D Discrete Element Method. The fluid phase flow equations are solved by the RiverFLO-2D computational model which is based on the 2D depth-averaged shallow water approximation and uses the Finite Element Method on a triangular non-structured mesh. The model considers particle-particle and wall-particle collisions, and considers that particles are immersed in a fluid and subject to gravity, friction and drag forces. Bingham and Cross rheological models are used for the continuum phase providing very stable results, even in the range of very low shear rates. Results show that the Bingham formulation proves better able to simulate the stopping of the fluid when applied shear stresses are low. Results from numerical simulations comparison with analytical solutions and data from flume-experiments, show that the model is capable of reasonable approximating the motion of large particles moving in the fluid flow. An application to simulate a debris flow event that occurred in Venezuela in 1999 shows that the model can model the main boulder accumulation reported for the alluvial fan in that event.

Key words: *debris flow, boulders accumulation, finite element method, discrete element method, lagrangian formulation*

INTRODUCTION

Debris flow is a frequently occurring phenomenon in mountainous regions. It occurs when masses of poorly sorted sediments, rocks and fine material, agitated and mixed with water, surge down slopes in response to water flow and gravitational attraction. A typical surge of debris flow has a steep front or "head" with the densest slurry, the highest concentration of boulders and the greatest depth. A progressively more dilute and shallower tail follows this head.

Reviews presented by Iverson (1997), exhaustively describe the physical aspects of debris flow motion and clearly divide previous debris flow research into two distinct categories. The first, based upon the pioneering work of Johnson (1965), assumes that debris flow behaves as a viscoplastic continuum. This model describes a single-phase material that remains rigid unless stresses exceed a threshold value: the plastic yield stress. Various rheological models have been proposed, derived from experimental results or from theoretical considerations, such as the Bingham model (Bingham & Green, 1919), the Cross model (Barnes *et alii*, 1989) and the quadratic model proposed by O'Brien & Julien (1985). The Bingham plastic model is the most commonly used in practice.

The second approach has focus on the mechanics

of granular materials. Based on BAGNOLD (1954), two-phase models have been developed by several authors, such as TAKAHASHI (1991) and IVERSON (1997). These models explicitly account for solid and fluid volume fractions and mass changes respectively.

Despite of the considerable progress over the past few years, the flow dynamics and internal processes of debris flows are still challenging in many aspects. In particular, there are many factors related to the movement and interaction of individual boulders and coarse sediments that have not been fully addressed in previous works. ASMAR *et alii* (2003) introduced the Discrete Element Method (DEM) to simulate the motion of solid particles in debris flows. DEM is a numerical method to simulate dry granular flows whereeach particle is traced individually in a Lagrangian frame ofreference by solving Newton's equation of motion.

This paper describes the development of a quasi threedimensional model to simulate stony debris flows, considering a continuum fluid phase, and large sediment particles, such as boulders, as a non-continuum phase. Large particles are treated in a Lagrangian frame of reference using DEM, and the fluid phase composed by water and fine sediments is modeled with an Eulerian approach using the depth-averaged Navier–Stokes equations in two dimensions. Bingham and Cross rheological models are used for the continuum phase. Particle's equations of motion are fully threedimensional. Numerical simulations have been compared with analytical solutions, with data from laboratory experiments and with a real debris flow event.

GOVERNING EQUATIONS

The flow domain is divided in computational cells with triangular base and depth H, as shown in Figure 1.

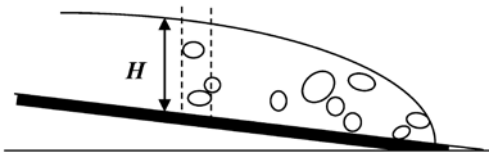

Fig. 1 - Schematic representation of debris flow with large solid particles

Assuming non-Newtonian and incompressible fluid phase, the depth averaged continuity and momentum equations in Cartesian coordinates can be written as follows:

$$\frac{\partial H}{\partial t}+\frac{\partial(\bar{u}H)}{\partial x}+\frac{\partial(\bar{v}H)}{\partial y}=0 \qquad (1)$$

$$\frac{1}{g}\frac{\partial \bar{u}}{\partial t}+\frac{\bar{u}}{g}\frac{\partial \bar{u}}{\partial x}+\frac{\bar{v}}{g}\frac{\partial \bar{u}}{\partial y}+\frac{\partial \eta}{\partial x}+\frac{F_{Dx}}{\rho g}+S_{fx}=0 \qquad (2)$$

$$\frac{1}{g}\frac{\partial \bar{v}}{\partial t}+\frac{\bar{u}}{g}\frac{\partial \bar{v}}{\partial x}+\frac{\bar{v}}{g}\frac{\partial \bar{v}}{\partial y}+\frac{\partial \eta}{\partial y}+\frac{F_{Dy}}{\rho g}+S_{fy}=0 \qquad (3)$$

where H is the water depth, η is the free-surface elevation, and and are the depth averaged velocities in x and y directions respectively; g is the gravitational acceleration and is fluid density. FD represents the fluid-solid interaction force exerted on the fluid by particles through the fluid drag force, this force is evaluated as:

$$\mathbf{F}_D=\frac{\sum_{i=1}^{n}\mathbf{F}_{FDi}}{\Delta V} \qquad (4)$$

where $F_{FD}i$ is the fluid drag force on each particle i, V is the volume of the computational cell and n is the number of particles in the cell.

S_{fx} and S_{fy} are the depth integrated stress terms that depend on the rheological formulation used to model the slurry. Assuming a Bingham rheological model and Manning's formula, as proposed by O'BRIEN & JULIEN (1985), the stress terms for the fluid can be expressed as

$$S_{fx} = \frac{\tau_y}{\rho g H} + \frac{3\mu\bar{u}}{\rho g H^2} + \frac{N^2 \bar{u}^2}{H^{4/3}} \quad (5)$$

$$S_{fy} = \frac{\tau_y}{\rho g H} + \frac{3\mu\bar{v}}{\rho g H^2} + \frac{N^2 \bar{v}^2}{H^{4/3}} \quad (6)$$

where N is the Manning roughness coefficient.

The fluid dynamic viscosity μ and yield stress y, are determined as functions of the volume sediment concentration Cv, using the relationships proposed by O'Brien & Julien (1988):

$$\mu = \alpha_1 e^{\beta_1 Cv} \quad (7)$$

$$\tau_y = \alpha_2 e^{\beta_2 Cv} \quad (8)$$

in which α_1, α_2 β_1 and β_2 are empirical coefficients obtained by data correlation in a number of experiments with various sediment mixtures.

Using a quadratic formulation combined with the Cross rheological model, the stress terms for the fluid are expressed as

$$S_{fx} = \frac{\mu_{eff}\dot{\gamma}}{\rho g H} + \frac{N^2 \bar{u}^2}{H^{4/3}} \quad \text{with} \quad \dot{\gamma} = \frac{3\bar{u}}{H} \quad (9)$$

$$S_{fx} = \frac{\mu_{eff}\dot{\gamma}}{\rho g H} + \frac{N^2 \bar{u}^2}{H^{4/3}} \quad \text{with} \quad \dot{\gamma} = \frac{3\bar{u}}{H} \quad (10)$$

where μ_{eff} is the effective viscosity of the fluid defined by:

$$\mu_{eff} = \frac{\mu_0 + \mu_\infty K_B \dot{\gamma}}{1 + K_B \dot{\gamma}} \quad (11)$$

$$\text{with} \quad K_B = \frac{\mu_0}{\tau_y}, \mu_\infty = \mu \text{ and } \mu_0 = 10^3 \mu \quad (11\,b)$$

In the solid phase, spherical particles of different diameters are considered. Particle trajectories are tracked using Newton's second law; considering gravity, buoyancy, fluid drag and collision forces.

$$m_i \frac{d\mathbf{v}}{dt} = \sum \mathbf{F}_E + \sum \mathbf{F}_N + \sum \mathbf{F}_T \quad (12$$

The external force $\mathbf{F}_E$ is given by

$$\mathbf{F}_E = \mathbf{F}_B + \mathbf{F}_{FD} \quad (13)$$

The expression to compute the net force acting on the particledue to gravitational effects is

$$\mathbf{F}_B = \frac{4}{3}\pi R^3 (\rho - \rho_p)\mathbf{g} \quad (14)$$

where R is the particle radius and ρ_p is the particle density.

The expression for the drag on particles in viscous fluid is given by

$$\mathbf{F}_{FD} = \frac{1}{2}\pi R^2 C_d \rho |\mathbf{u} - \mathbf{v}|(\mathbf{u} - \mathbf{v}) \quad (15)$$

where C_d is the drag coefficient, **u** is the fluid velocity vector at the particle location, and **v** is the particle velocity vector.

The last two terms in equation (12) represent the collision forces or contact forces among particles. Based on the simplified model that uses a spring-dashpot-slider system to represent particle interactions (Asmar *et alii*, 2003), the normal contact force and the tangential contact force are evaluated as

$$\mathbf{F}_N = \mathbf{F}_{NC} + \mathbf{F}_{ND} \quad (16)$$

$$\mathbf{F}_T = \mathbf{F}_{TC} + \mathbf{F}_{TD} \quad (17)$$

The normal contact force F_{NC} is calculated using a Hook's linear spring relationship,

$$\mathbf{F}_{NC} = K_N \delta_N \quad (18)$$

where K_N is the normal contact stiffness and δ_N is the displacement overlap) between particles *i* and *j*. The maximum overlap is dependent on the stiffness K_N. Typically, average overlaps of 0.1-1.0% are desirable, requiring stiffness of the order 105-107 N/m.

The normal damping force $\mathbf{F}_{ND}$ is also calculated using a linear relation given by

$$\mathbf{F}_{ND} = C_N \boldsymbol{v}_N \tag{19}$$

where v_N is the normal component of the relative velocity between particles and C_N is the normal damping coefficient. This constant C_N is chosen to give a required coefficient of restitution β, defined as the ratio of the normal component of the relative velocities before and after collision.

The tangential contact force, $\boldsymbol{F}_{TC}$, represents the friction force and it is constrained by the Coulomb frictional limit, at which point the particles begin to slide over each other. Prior to sliding, the tangential contact force is calculated using a linear spring relationship,

$$\mathbf{F}_{TC} = K_T \delta_T \tag{20}$$

where K_T is the tangential stiffness coefficient, and δ_T is the total tangential displacement between the surfaces of particles *i* and *j* since their initial contact. When $K_T\,\delta_T$ exceeds the frictional limit force $\mu_f F_{NC}$, particle sliding occurs. The sliding condition is defined as

$$\mathbf{F}_{TC} = \mu_f \mathbf{F}_{NC} \tag{21}$$

where μ_f is the dynamic friction coefficient.

The tangential damping force $\mathbf{F}_{TD}$ is not included in this model, since it is assumed that once sliding occurs, damping is accounted for from friction. Particle rotation is not considered, since it its impact on boulder transport is assumed to be of much less importance than the friction and drag forces.

Since the fluid phase governing equations are depth integrated, gradients along z direction are equal to zero in the formulation, as well as the velocity in this direction, *w*. Then, torque in *x* and *y* directions are not detectable by the numerical model. Last component is the torque in direction perpendicular to the sloping surface, which is essentially negligible.

Fluid governing equations (1-3) are solved by the Galerkin Finite Element method using three-node triangular elements. To solve the resulting system of ordinary differential equation, the model applies a four-step time stepping scheme and a selective lumping method, as described by Garcia-Martinez *et alii*. (2006).

Forces on each particle are evaluated at each time step, and the acceleration of the particle is computed from the particle governing equation, which is then integrated to find velocity and displacement of each particle.

RESULTS

ANALYTICAL SOLUTIONS

The first modeling step was the implementation of different rheological models for the simulation of mud flows. This modeling would account for the representation of the fluid phase of the debris flow. The numerical model was run using RiverFLO-2D software, a finite modeling system for detailed analysis of river hydrodynamics, sediment transport and bed evolution (García-Martínez *et alii*, 2006). In the software, two rheological quadratic formulations were implemented, the first, including Bingham theory and Manning's formula, as proposed by O'Brien & Julien in 1985, and the second, combining Cross formulation and the Manning's formula as proposed in Martinez *et alii* (2007).

In order to compare with simple results, an analytical solution, proposed by Huang & Garcia (1997), was studied and implemented in a computer program. This implementation provided enough data for verification and testing of the new rheological formulations proposed (Martinez *et alii*, 2007).

LABORATORY EXPERIMENTS

A series of experiments were carried out in a laboratory flume, using homogeneous fine sediment mixtures for the continuum phase and spherical marbles for the discrete phase. The experiments were performed in a 1.9 m long, 0.19 m wide, Plexiglas walled flume, with adjustable slope. The downstream

part of the flume was connected to a wood horizontal platform, 0.75 m long and 0.95 m wide. A dam-break type of flow was initiated by an abrupt removal of a gate, releasing mixtures from a 0.40 m long reservoir situated on the upstream part of the flume. Water-clay mixtures were used in all the experiments, with volume sediment concentration 23.5 % and 26.5 %. For preparation of the mixtures, kaolinite clay with specific unit weight of 2.77 was used. Fluid density was measured in the laboratory and rheological parameters μ and τ_y were determined using equations (7) and (8) in which parameters are $\alpha_1 = 0.621 \text{x} 10^{-3}$, $\beta_2 = 17.3$, $\alpha_2 = 0.002$ and $\beta_2 = 40.2$.

Fig. 2 - Experiment 1, fluid stops flowing over the sloping channel

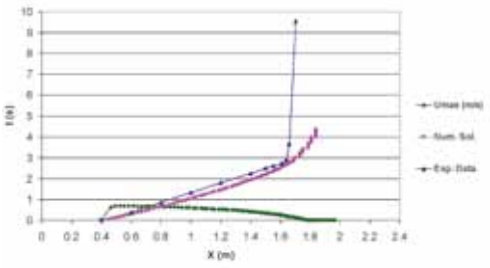

Fig. 3 - Experiment 1, spreading relation

Cv (%)	ρ (Kg/m^3)	μ (Pa.s)	τ_y (Pa)
23.5	1410	0.0362	25.34
26.5	1460	0.0608	84.64

Tab. 1 - Rheological properties of experimental fluids

EXPERIMENT 1

In this experiment the flow of a mixture of 23.5% volume concentration was studied. The flume bottom slope was set to 4° and the initial volume released was 6.3 L. For $t = 3$ s the wave practically stopped flowing as shown in Fig. 2. The propagation of the wave was recorded for different times t to construct the spreading diagram shown in Fig. 3.

Figure 3 compares the experimental data with the numerical solution using Bingham rheological formulation. Numerically, the condition of stopping the fluid is not easy to achieve; however, it is possible to appreciate how the maximum velocity in the fluid decreases with time and it becomes very close to zero about the time the fluid must stop. This fact shows that velocity criteria could be used numerically to stop the fluid.

….The following two figures compare longitudinal profiles and maximum velocity for two different mesh sizes. Figures 4 and 5 show how mesh refinement contributes to improve substantially the

solution in the advancing front. The wet-dry algorithm proposed by Garcia *at alii* (2009) was implemented to eliminate dry elements from the calculation, and then there is a well defined interface between dry and wet elements.

However, there is a numerical tendency to form a spurious low depth front that that could be reduced

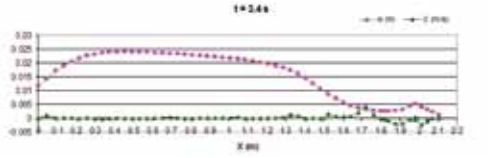

Fig. 4 - Final free-surface longitudinal profile and U_{max} - mesh size 0.03 m

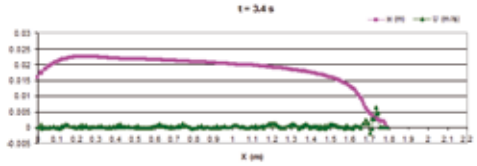

Fig. 5 - Final free-surface longitudinal profile and Umax - mesh size 0.01 m

decreasing the element size as well as reducing the minimum depth parameter that determines the distinction between dry and wet elements. Best results were found with a minimum depth parameter equal to 0.01 times the average fluid depth as shown in Fig. 5.

EXPERIMENT 2

In this experiment the same mixture as in experiment 1 is used. In this case, the flume bottom slope was set to 9.54° and the initial volume released was 6.4 L. The objective of this test was to study the spreading of the fluid in the fan and to study particle movement into the fluid.

Fourteen particles, with diameter 2.5 cm and density 2500 kg/m^3, were placed in two rows over a small piece of wood in the mud reservoir, just behind the gate. By the time the fluid was released, the piece of wood was quickly removed, so the particles could start their movement along the channel with the fluid

Figure 6(a) shows the particles resembling the velocity parabolic distribution across the channel at t = 0.5 s. Blue particles represent those particles placed initially in the first row, orange particles are those placed in the second row. In Figure 6(b) can be noticed how particles in the center tend to move forward to reach the front of the wave, particles in the second row displace particles in the first row to the sides and these are then left behind because of the fluid velocity gradient. By the time the flow reaches the fan, particles move to the sides of the flow as it is shown in Figure 7.

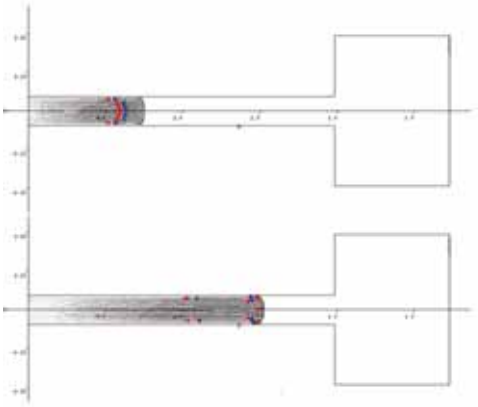

Fig. 6. - Experiment 2, numerical simulation (a) t = 0.5 s, (b) t = 1.6 s

Figure 7 compares final position of particles obtained experimentally (final position of particles was measured at the lab) with the numerical results. In the numerical solution can be seen that there exist some delay on the particles positioned close to the walls; this is due to the velocity boundary condition at the walls. In practical applications of the model, it is necessary to allow slip at the walls, since the no slip condition formulated in finite elements becomes very restrictive. However; it is not possible a total slip condition, since for this case no velocity profile would be created across the channel. In this simulation 90% of slip at the wall was considered.

EXPERIMENT 3

In this experiment, a mixture of volumetric concentration of 26.5% was studied. In this case, the flume bottom slope was increased to 10.7° and the initial volume released was 11.1 L. The objective of this test was to study the spreading of the fluid and study particle movement into a mixture with higher clay concentration.

Figure 8 shows the spreading relation in the lon-

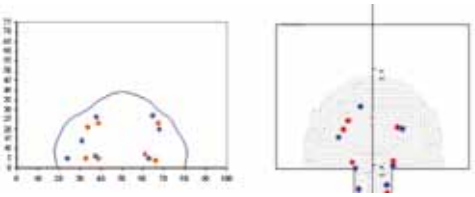

Fig. 7 - Experiment 2: Final position of particles (a) experimental data(b) numerical solution

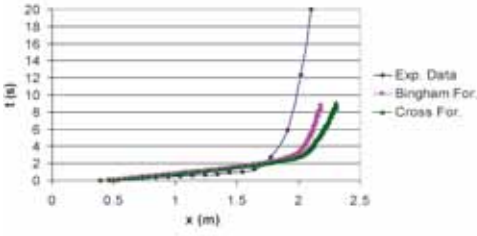

Fig. 8 - Experiment 3, spreading relation

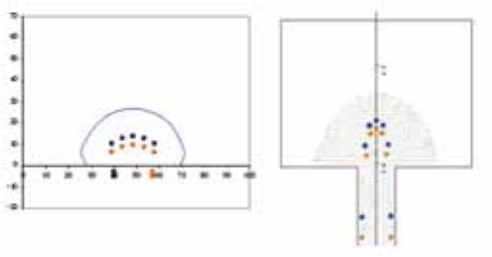

Fig. 9 - Experiment 3: Final position of particles, (a) experimental data(b) numerical solution

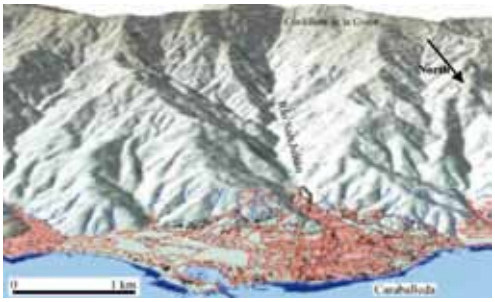

Fig. 10 - Caraballeda alluvial fan, Venezuela

gitudinal direction for this experiment. This relation is compared with numerical results obtained using Bingham rheological model and using Cross rheological model. Both rheological formulations produce very similar results, they are not totally capable of resembling the spreading of the flow; however, they show a final fluid extend, when velocities in the fluid become very close to zero, very similar to the real one. Bingham formulation shows to be more effective in decreasing the velocities oalong the fluid to zero.

In this experiment 14 particles were placed on the fluid in a similar manner that was done in the previous experiment. Figure 9 compares the final particle positions obtained numerically against final observed particle location. Note that some particles lag behind close to the flume wall and that the general location of the particles on the alluvial fan is very close to the observed locations.

.

APPLICATION: VENEZUELA'S 1999 ALLUVIAL FAN DEBRIS FLOODING EVENT

Heavy rainfall from a storm on December 14-16, 1999, triggered thousands of shallow landslides on steep slopes of Cerro El Avila, north of Caracas, Venezuela, and caused flooding and massive debris flows in the channels of major drainages that severely damaged coastal communities along the Caribbean Sea. The largest fan on this area is that of San Julián River at Caraballeda, shown in Figure 10. This fan was one of the most heavily damaged areas in the event. The thickness of sediment deposition, maximum size of transported boulders, and size of inundated area were all notably larger in this drainage in comparison to the other close watersheds.

The US Geological Survey studied the affected area (Wieczorek *et alii*, 2001), measuring slope, deposit thickness, and boulder size from the fan apex to the distal end of the fan near the coastline. Data was used to map the distribution and thickness of deposits and to draw contours of maximum boulder size, as shown in Figure 11.

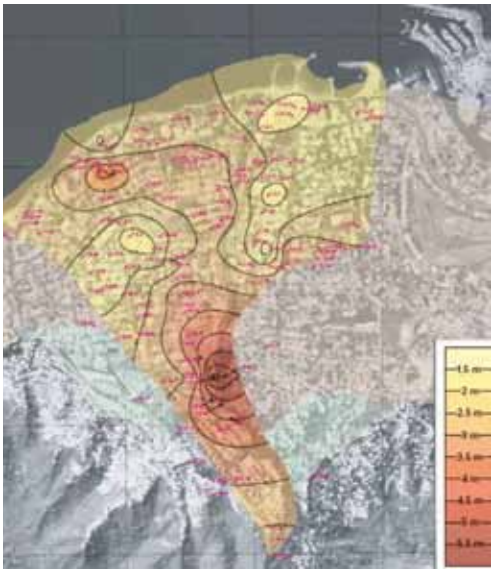

Fig. 11 - Contours of maximum transported boulder size on the Caraballeda alluvial fan, Venezuela. From USGS, 2002

The numerical simulation was performed using a finite element mesh with 22,500 triangular elements. The element characteristic size was 12 m on average. The topography data used to define the finite element mesh was interpolated from the original cartographic information prior to the event (Garcia, 2008).

A 500 year-return period hydrograph was used as flow input at the fan apex, as shown in Figure 12, with an average volume sediment concentration of Cv=0.3. The Manning coefficient considered

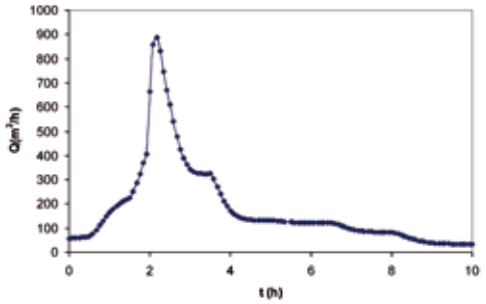

Fig. 12 - Inflow hydrograph for a 500 year-return period, including solid concentration by volume of 0.3

was equal to 0.065 in the whole fan area, in order to take into account terrain irregularities. The same value was used by Garcia (2008), and was found a good estimate for the area. The empirical relationships (7) and (8) were selected for the calculation of fluid rheological properties, using the parameters for water-clay mixtures. As a result of the volume sediment concentration, Cv = 0.3, ρ = 1531 kg/m^3, μ = 0.11 Pa.s, τ_y = 105 Pa.

During the simulation, 1600 boulders with sizes ranging from 1 m to 6 m in diameter were included in the event. The boulders were placed into the fan during the first three hours of simulation, at a rate of 50 particles every 6 min. This amount of particles was selected to ensure a manageable computational time. Density for the boulders is ρ_p = 2600 kg/ m^3, equal to the density of Gneiss boulders, the type of boulders mostly found in the area by the USGS.

Figure 13 shows the flooded area at time t = 2.2 h, the time corresponding with the peak discharge in Figure 12. Comparing this region with the post-event aerial view shown in the background, it can be noted that the model acceptably reproduces the extent of the area affected by the debris flow.

Figure 14 shows the velocity field at time t = 2.2 h. It can be seen that major velocities occurs in the fan apex, where the discharge of the river is simulated. Velocities decrease at the urban areas, ranging from 1.0 to 6 m/s at the time of the hydrograph maximum value. Higher velocities are developed in the avulsion zone, at the center of the fan,, reaching 10 m/s. The velocities calculated by the model are in good agreement with those estimated by USGS, which ranged from 1.3 to 13.6 m/s.

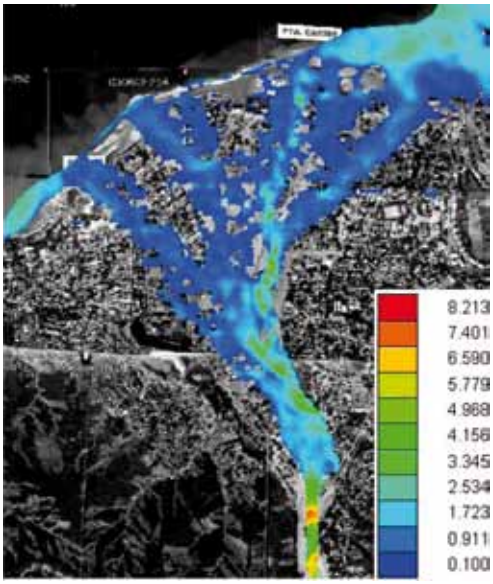

Fig. 13 - Flooded area at time t =2.2 h. Legend indicates flow depth in m

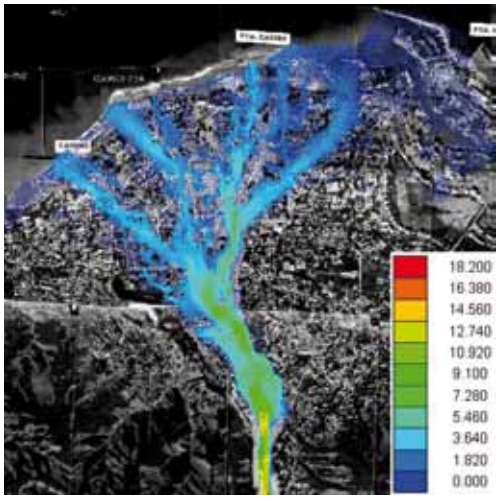

Fig. 14 - Velocity field at t =2.2 h. Legend indicates velocity in m/s

Figure 15 shows how boulders, are transported by the flow along the main drainage paths.

It is interesting to note how the largest boulders follow the path of the original concrete channel toward the right side of the fan, while smaller boulders take the central path. According to the USGS report, the slope at the center was 4 degrees, while the concrete channel direction, was steeper, with a slope gradient of 5.5 to 6 degrees, then larger boulders were trans-

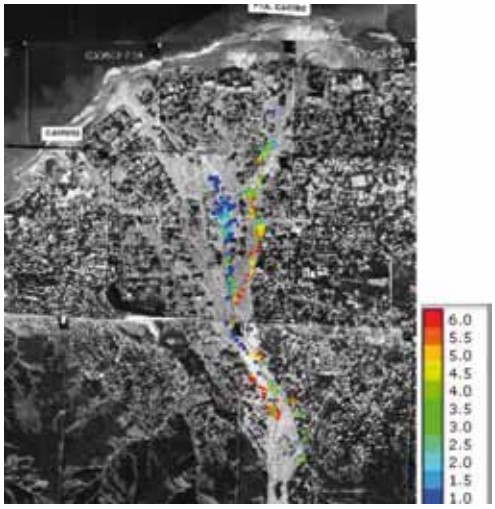

Fig. 15 - Boulder positions at time t =1.8 h, Legend indicates particle diameter in m

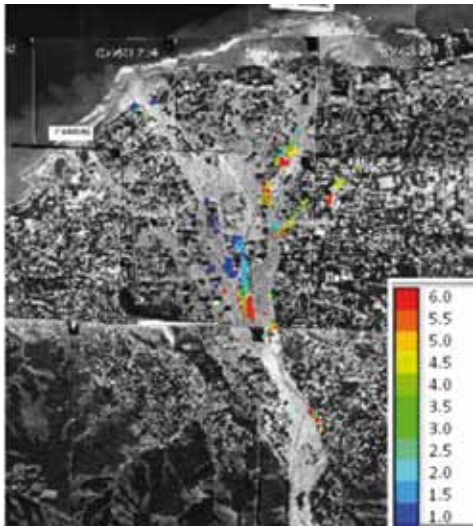

Fig. 16 - Boulder positions at time t = 6.0 h, Legend indicates particle diameter in m

ported to this side. These values of mean nominal diameter and slope steepness reflect USGS observations that for the larger transported and deposited boulders there was a proportional relationship between boulder size and slope steepness.

Figure 16 shows boulder positions after 6 hours of simulation. Smaller boulders continue taking the central direction alignment, some of them reached the shoreline or entered into the sea. Larger boulders were deposited in the avulsion zone or took right direction to the concrete channel. None of these large boulders reached the shoreline. In Figure 16, it can be seen that the model predicts reasonably boulder locations as compared with the field data given in Figure 11.

According to USGS, the largest boulders were found in the avulsion zone, within a thick matrix, evidence that strongly supports transport by debris flow. At other sites, the largest boulders were observed isolated along the concrete channel, fact that suggests that these boulders moved sliding along the bottom of the channel in a dilute fluid until deposition occurred (USGS Report 01-0144). There is no indication of big boulders close to the shoreline at this site of the fan.

According to Takahashi (1991), during the process of deposition, debris flows deposit the boulders in order from bigger to smaller as it proceeds downstream on alluvial fans. This process was better observed along the central direction and it was also replicated in the numerical simulation.

CONCLUSIONS

This paper describes the development and application of a quasi three-dimensional two-phase model to simulate debris flows, considering large particles, such as boulders. The continuum non-Newtonian phase is solved by RiverFLO-2D finite element model in two horizontal directions and the particle transport with the Discrete Element Method in 3D.

The model is able to simulate fluid and particle transport when compared against several experiments in a laboratory flume-fan, including the effect of particle-particle and wall-particle collisions.

Bingham and Cross rheological formulations provide very stable results, even in the range of very low shear rates. In the simulation of mud dam-break problems, Bingham formulation was better able to simulate the stopping stage of the fluid; however, the Cross formulation proved more accurate for early stages of the solution.

An application to the well documented debris flow event that occurred in Venezuela in 1999 illustrates the capability of the model to simulate large scale real events. Results show that the model reasonably approximates the flood extent affected by the debris flow and the observed boulder accumulation areas, including distribution boulders sizes. Future work includes comparison with field events using larger number of boulders and enhancement of the detecting particle contact algorithm in order to improve computational time.

REFERENCES

Asmar B.N., Langston, P.A. & Ergenzinger P. (2003) - *The potential of the Discrete Element Method to simulate debris flow.* Debris-flow hazards mitigation: mechanics, prediction and assessment, **1**: 435-445.

Bagnold R. A. (1954) - *Experiments on a gravity-free dispersion of large solid spheres in a Newtonian fluid under shear.* Proceedings of the Royal Society of London, **225**: 49-63.

Barnes H.A., Hutton J.F. & Walters K. (1989) - *An introduction to rheology.* Elsevier. Amsterdam.

Bingham E.C. & Green H. (1919) - P*aint a plastic material and not a viscous liquid; the measurement of its mobility and yield value.* Proceedings of American Society of Testing Materials, **19**: 640-664.

García-Martínez R., Espinoza R., Valera E. & González M. (2006) - A*n explicit two-dimensional finite element model to simulate short and long term bed evolution in alluvial rivers.* J. of Hyd. Res., **44**(6): 755-766.

Garcia-Martínez R. (2002) - M*ud Flow Hazard Maps for Vargas State. Final Report for the Avila Project.* Fluid Mechanics Institute, University Central of Venezuela (In Spanish).

Garcia-Martínez R., Gonzalez N. & O'Brien J. (2009) - *Dam-break flood routing.* Chapter 5 of Dam-Break Problems, Solutions and Case Studies. Ed. De Wrachien, D. & Mambretti, WIT Press. ISBN: 978-1-84564-142-9.

Iverson R.M. (1997) - *The physics of debris flows*. Rev. of Geophysics, **35**: 245-296.

Johnson A.M. (1965) - A model for debris flow. Ph.D. dissertation. Pennsylvania State University, University Park.

Martinez C., Miralles-Wilhelm F. & Garcia-Martinez R. (2007) - *A 2D finite element debris flow model based on the cross rheology formulation.* Fourth International Conference on Debris-Flow Hazards Mitigation: Mechanics, Prediction and Assessment. Chendu, China.

O'Brien J.S. & Julien P.Y. (1985) - *Physical properties and mechanics of hyperconcentrated sediment flows.* ASCE Specialty Conference on the Delineation of Landslides, Debris Flows Hazards, 260-279.

O'Brien, J.S. & Julien, P.Y. (1988) - *Laboratory analysis of mudflows properties.* J. of Hyd. Eng., **114**(8): 877-887.

Takahashi T. (1991) - *Debris Flows.* Balkema, Rotterdam.

Wieczorek G.F., Larsen M.C., Eaton L.S., Morgan B.A. & Blair J. L. (2001) - *Debris-flow and flooding hazards associated with the December 1999 storm in coastal Venezuela and strategies for mitigation*. U.S. Geological Survey, Open File Report 01-0144.